Power-balanced dynamic modeling of vactrols: application to a VTL5C3/2

Judy Najnudel, Müller Remy, Thomas Hélie, David Roze

POWER-BALANCED DYNAMIC MODELING OF VACTROLS: APPLICATION TO A VTL5C3/2

Judy Najnudel and Rémy Müller

UVI
Paris, France
j.najnudel@uvi.net | r.muller@uvi.net

Thomas Hélie and David Roze

IRCAM-CNRS-SU
Paris, France
thomas.helie@ircam.fr | david.roze@ircam.fr

ABSTRACT

Vactrols, which consist of a photoresistor and a light-emitting element that are optically coupled, are key components in optical dynamic compressors. Indeed, the photoresistor's program-dependent dynamic characteristics make it advantageous for automatic gain control in audio applications. Vactrols are becoming more and more difficult to find, while the interest for optical compression in the audio community does not diminish. They are thus good candidates for virtual analog modeling. In this paper, a model of vactrols that is entirely physical, passive, with a program-dependent dynamic behavior, is proposed. The model is based on first principles that govern semi-conductors, as well as the port-Hamiltonian systems formalism, which allows the modeling of nonlinear, multiphysical behaviors. The proposed model is identified with a real vactrol, then connected to other components in order to simulate a simple optical compressor.

1. INTRODUCTION

A vactrol (or resistive opto-isolator) consists of a photoresistor (labelled LDR for Light-Dependent Resistor in the following) and a light-emitting element (usually a LED) that are optically coupled: the photoresistor's resistance decreases (nonlinearly) with the light it receives from the LED.

Vactrols were widely used from the 1960s to the early 2000s due to their low fabrication costs, important dynamic range, and low noise distortion (below - 80 dB). They could be found in cameras (in exposure meters and autofocus) and security systems (for object detection) to name a few applications.

Apart from their nonlinear response to light, a remarkable feature of photoresistors is their relatively long response times (compared to e.g. transistors in transistor opto-isolators). Indeed, these response times vary from a few tens of microseconds (for the *turn-on*, or attack, when light is switched on) to a few hundreds of milliseconds (for the *turn-off*, or release, when light is switched off). Moreover, the attack time decreases with the received light. These characteristics made vactrols much appreciated for automatic gain control in audio applications, in which adaptive treatment and transient preservation are essential. An emblematic example of optical dynamic compressors from the late 1960s is the LA-2A built by Teletronix [1], which was used in prominent broadcast studios such as CBS and RCA. A more recent example is the Langevin ELOP built by Manley [2].

Vactrols were manufactured by Perkin Elmer [3] among others, until 2010. They are still manufactured by Advanced Photonix, but their availability has severely diminished since the 2000s due to a EU ban on cadmium sulfide, which is one of the main components of photoresistors. As vintage optical dynamic compressors are priced at tens of thousands of dollars, an accurate simulation is a convenient and much cheaper way to access optical dynamic compression.

Models of vactrols for audio applications have been proposed in the literature [4, 5]. Based on a signal representation, they associate static characteristics obtained from measurements, and a combination of low-pass filters to account for the photoresistor's dynamic behavior. More recent models based on Recurrent Neural Networks [6, 7] allow the joint inference of static and dynamic characteristics from data.

Although these models demonstrate interesting features from both qualitative and computational points of view, they are tailored to a specific circuit; therefore, they offer much less modularity than purely physical models. In particular, they are difficult to connect to other components modeled as port-Hamiltonian systems, which provide a unified formalism for the modeling of multiphysical systems with passivity guarantees, and has proven relevant for audio applications [8, 9]. Moreover, a key specificity of vactrols, namely, the inherent *program-dependence* of the attack and release times, remains elusive in signal-based models.

In this paper, which is a condensed version of the work presented in [19], we propose a nonlinear model of vactrols that is entirely physical, passive, with a program-dependent dynamic behavior by construction. To this end, we rely on first principles that govern semi-conductors, and the port-Hamiltonian systems (PHS) formalism.

This paper is structured as follows. In Section 2, we give a brief reminder on PHS. In Section 3, we recall the main doping mechanisms in photoresistors and derive a model for their internal dynamics. Then in Section 4, we propose a law for the optical coupling between the LED and the photoresistor, and obtain a complete PHS model for the vactrol by connecting all subcomponents through multiphysical ports. Finally, the model's parameters are estimated from measurements of a real vactrol, and then used to simulate a simplified optical compressor in Section 5.

2. REMINDER ON PORT-HAMILTONIAN SYSTEMS

Any physical system can be divided into parts that interact with each other via energy exchanges. Detailed presentations of PHS are available in [10, 11, 12]. In this paper, we rely on a differential-algebraic formulation adapted to multiphysical systems [13, 14]. This formulation allows the representation of a dynamical system as a network of

1. storage components of state $\boldsymbol{x}$ and energy $E(\boldsymbol{x})$;
2. passive memoryless components described by an effort law $z : \boldsymbol{w} \mapsto z(\boldsymbol{w})$, such that the dissipated power $P_{\text{diss}} = z(\boldsymbol{w})^\intercal \boldsymbol{w}$ is non-negative for all flows $\boldsymbol{w}$;
3. connection ports conveying the *outgoing* power $P_{\text{ext}} = \boldsymbol{u}^\intercal \boldsymbol{y}$ where $\boldsymbol{u}$ are inputs and $\boldsymbol{y}$ are outputs.

The system flows $\boldsymbol{f}$ and efforts $\boldsymbol{e}$ are coupled through a (possibly dependent on $\boldsymbol{x}$) skew-symmetric interconnection matrix $\boldsymbol{S} = -\boldsymbol{S}^\intercal$, so that

$$\underbrace{\begin{bmatrix}\dot{\boldsymbol{x}}\\ \boldsymbol{w}\\ \boldsymbol{y}\end{bmatrix}}_{\boldsymbol{f}} = \boldsymbol{S} \underbrace{\begin{bmatrix}\nabla E(\boldsymbol{x})\\ z(\boldsymbol{w})\\ \boldsymbol{u}\end{bmatrix}}_{\boldsymbol{e}}. \tag{1}$$

In the context of electronic circuits, flows can either be currents (e.g. for capacitors) or voltages (e.g. for inductors), and vice versa for efforts.

Such systems satisfy the power balance

$$P_{\text{stored}} + P_{\text{diss}} + P_{\text{ext}} = 0 \tag{2}$$

where $P_{\text{stored}} = \nabla E(\boldsymbol{x})^\intercal \dot{\boldsymbol{x}}$ denotes the stored power.

Proof By skew-symmetry of $\boldsymbol{S}$ (which we recall diagonal is zero),

$$P_{\text{stored}} + P_{\text{diss}} + P_{\text{ext}} = \boldsymbol{e}^\intercal \boldsymbol{f} = \boldsymbol{e}^\intercal \boldsymbol{S} \boldsymbol{e} = 0. \quad \square$$

Note that throughout this paper, we adopt the *receiver convention* for all components, including external sources. This means that the current is defined positive when entering the component through the positive voltage terminal [15].

3. PHOTORESISTOR

A photoresistor consists of a thin layer of photoconductive material (typically, cadmium sulfide) deposited on a ceramic substrate. In the following, we assume that the photoconductive material is spatially homogeneous, so that no pn-junction can be formed and that diffusion of free carriers is negligible. As a consequence, the photoresistor internal dynamics can be modeled by ODEs.

A photoresistor is in fact a 2-port component. The first port is electrical, and allows connections to other electronic components like any other resistor. The second port is optical, and allows interactions with light. It is responsible for internal dynamics in the micro-electrical domain. In the next sections, the (hidden) flow and effort that result from optical interactions are explicitly referred to as f_{opt} and e_{opt}, to avoid confusion with the (directly observable) electrical flow i_{LDR} (current), and electrical effort v_{LDR} (voltage). Note that both flows are in Amperes, and both efforts are in Volts.

3.1. Photoconductivity and doping

Photoconductive materials are semiconductors, that is, they become conductive under certain conditions. Indeed, the photoabsorption of a small amount of additional energy (denoted e_g) generates a pair of free carriers: an electron in the conduction band (of energy E_C), and a hole in the valence band (of energy E_V). The presence of free carriers increases the photoresistor conductivity. Note that the overall conductivity depends on the quantity of electrons, but also on the quantity of holes (which, as we shall see, do not necessarily remain equal).

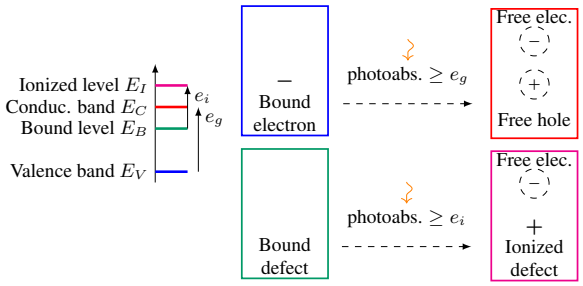

Figure 1: *Energy levels and free carriers before and after photoabsorption for an n-doped semi-conductor.*

The conductivity of a photoconductive material can be artificially increased (or "doped") through the inclusion of defects, which lower the amount of energy needed to generate free carriers via ionization [16]. Here, we consider n-doped materials only, as cadmium sulfide (which is present in Vactrols) is most generally n-doped [17]. For efficient n-doping, the bound defect energy (denoted E_B) must lie between the valence band and the conduction band, and the ionized defect energy (denoted E_I) must lie in the conduction band, so that the ionization energy e_i is smaller than e_g and electrons reach the conduction band more easily (Fig. 1).

3.2. Internal dynamics

The internal dynamics of the photoresistor is due to carrier recombination processes. The most important recombination process in doped materials is the Shockley-Read-Hall recombination [16], in which free carriers recombine with defects. Therefore, other kinds of recombination (e.g., radiative and Auger) are neglected.

The Shockley-Read-Hall recombination can be summed up as follows (Fig. 2). Assume an initial state with no free carriers, denoted s_0. Photoabsorption can lead either to ionization (state s_i), or to electron-hole pair generation (state s_g). The ionized defect can then return to state s_0, followed by the dissipation of excess energy e_i. In this case, the ionized defect acts as a "trap" for electrons. Likewise, an electron-hole pair can recombine to state s_0, followed by the dissipation of excess energy e_g.

For convenience, and since this is transparent energy-wise, we choose to model a unique source of photoabsorption (that leads to electron-hole pair generation), and replace a transition from state s_g to state s_0, followed by a transition from state s_0 to state s_i, with a direct transition from state s_g to state s_i, that dissipates the energy $e_g - e_i$. In this case, the bounded defect acts as a "trap" for holes.

Free carriers dynamics modeling To model the free carriers dynamics in the micro-electrical domain, we rely on the homogeneous Iverson model [18]. Denote f_{opt} the optical flow responsible for the generation of free carriers (in receiver convention), q^- the absolute charge of electrons and $\dot{q}^-$ its time variation, q^+ the absolute charge of holes and $\dot{q}^+$ its time variation, q_τ^+ the absolute charge of defects in ionized state, q_τ^0 the absolute charge of defects in bound state[1], and q_τ the absolute charge of defects. The photoresistor internal dynamics are governed by the following

[1] Here, the absolute charge of a species is to be understood as the number of instances multiplied with the elementary charge for homogeneity. Therefore, it can be non-zero even for bound defects.

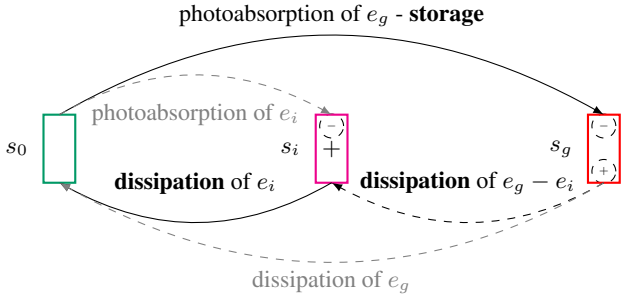

Figure 2: *Possible states and transitions for a n-doped photoresistor with Shockley-Read-Hall recombination. For convenience, a transition from state s_g to state s_0 followed by a transition from state s_0 to state s_i (gray, dashed), is replaced by a transition from state s_g to state s_i (black, dashed).*

equations [16]:

$$\text{Electron charge variation} \qquad \dot{q}^- = -f_{\text{opt}} - \nu_0^- \, q_\tau^+ \, q^-, \tag{3a}$$

$$\text{Hole charge variation} \qquad \dot{q}^+ = -f_{\text{opt}} - \nu_0^+ \, q_\tau^0 \, q^+, \tag{3b}$$

$$\text{Constant quantity of defects} \qquad q_\tau = q_\tau^+ + q_\tau^0, \quad \dot{q}_\tau = 0, \tag{3c}$$

$$\text{Charge neutrality} \qquad q_\tau^+ + q^+ - q^- = 0, \tag{3d}$$

where the electron (resp. hole) absolute charge time variation corresponds to the free carriers generation rate minus the de-ionization (resp. ionization) rate. The constants ν_0^- and ν_0^+ (in $\text{C}^{-1}{\cdot}\text{s}^{-1}$) relate to the electron and hole velocity, respectively. The constraints expressed by Eqs. (3c)-(3d) allow the reduction of Eqs. (3a)-(3b) to

$$\dot{q}^- = -f_{\text{opt}} - \nu_0^- \left(q^- - q^+\right) q^-, \tag{4a}$$

$$\dot{q}^+ = -f_{\text{opt}} - \nu_0^+ \left(q_\tau + q^+ - q^-\right) q^+. \tag{4b}$$

PHS formulation and equivalent circuit The system described by Eq. (4) admits a PHS formulation. To give this system a physical interpretation in terms of currents and voltages, we introduce capacities C^+ and C^-, as well as conductances $G_\tau^-(q^+, q^-) := \nu_0^- \, C^- \left(q^- - q^+\right)$ and $G_\tau^+(q^+, q^-) := \nu_0^+ \, C^+ \left(q_\tau + q^+ - q^-\right)$. The internal dynamics of the photoresistor can thus be described by two equivalent capacitors C^- and C^+ that model the storage of electrons and holes respectively, with flow $\dot{\boldsymbol{x}}$ (in Amperes) and effort $\nabla E(\boldsymbol{x})$ (in Volts)

$$\begin{aligned} \dot{\boldsymbol{x}} &= \left[\dot{q}^+, \dot{q}^-\right]^\intercal =: \left[f_{\text{C}+}, f_{\text{C}-}\right]^\intercal, \\ \nabla E(\boldsymbol{x}) &= \left[\frac{q^+}{C^+}, \frac{q^-}{C^-}\right]^\intercal =: \left[e_{\text{C}+}, e_{\text{C}-}\right]^\intercal, \end{aligned} \tag{5}$$

and two conductors G_τ^- and G_τ^+ that model the dissipation caused by de-ionization and ionization respectively, with flow $\boldsymbol{w}$ (in Volts) and (state-modulated) effort $z(\boldsymbol{w})$ (in Amperes)

$$\boldsymbol{w} = \left[e_{G_\tau^+}, e_{G_\tau^-}\right]^\intercal, \quad z(\boldsymbol{w}) = \left[G_\tau^+ \, e_{G_\tau^+}, G_\tau^- \, e_{G_\tau^-}\right]^\intercal =: \left[f_{G_\tau^+}, f_{G_\tau^-}\right]^\intercal. \tag{6}$$

The schematics of the corresponding equivalent circuit is shown on Fig. 3a, with corresponding PHS equations in Fig. 3b.

Remark 1. *The dynamics described by Eq. (4) depends on $C^\pm$ through the reduced parameters $\nu_0^\pm = \nu_0^\pm \, C^\pm \cdot \frac{1}{C^\pm}$. As only $\nu_0^\pm$ have to be identified and $\nu_0^\pm \, C^\pm$ and $C^\pm$ are unknown, we arbitrarily set $C^+ = C^- = 1$ F.*

Photoresistor electrical flow and effort The resistance of the photoresistor is given by [16]

$$R(q^+, q^-) = \frac{1}{\mu_0^+ \, q^+ + \mu_0^- \, q^-}, \tag{7}$$

where μ_0^+ (resp. μ_0^-) is the surface mobility (in $\text{V}^{-1}{\cdot}\text{s}^{-1}$) of holes (resp. electrons) and relates to the dimensions of the photoresistor and the mobility of holes.

In practice, the photoresistor exhibits a large but finite positive resistance R_d when it is not exposed to light (d for *dark*), and a small but non-zero positive resistance R_ℓ when it is exposed to maximal light (ℓ for *light*). The total resistance $R_{\text{LDR}}(q^+, q^-)$ is thus modeled as a parallel/series interconnection governed by

$$R_{\text{LDR}}(q^+, q^-) = \frac{R_\text{d}\left(R(q^+, q^-) + R_\ell\right)}{R_\text{d} + R(q^+, q^-) + R_\ell}. \tag{8}$$

As R_d is several orders of magnitude larger than R_ℓ, it is immediately verified that $\lim_{R \to +\infty} R_{\text{LDR}} = R_\text{d}$ and $\lim_{R \to 0} R_{\text{LDR}} = R_\ell$. We deduce the electrical flow $\boldsymbol{w}$ and (state-modulated) effort $z(\boldsymbol{w})$ of the photoresistor:

$$\boldsymbol{w} = i_{\text{LDR}}, \quad z(\boldsymbol{w}) = R_{\text{LDR}}\left(q^+, q^-\right) i_{\text{LDR}} =: v_{\text{LDR}}. \tag{9}$$

4. OPTICAL COUPLING

4.1. Power conversion between the LED and the photoresistor

Two types of power conversion take place between the LED and the photoresistor. The first one is a conversion from electrical to optical and occurs during photoemission by the LED. The second one is a conversion from optical to micro-electrical and occurs during photoabsorption by the photoresistor.

However, as the photoresistor spectral sensitivity does not match exactly with the LED spectral output, some of the power emitted by the LED is not transmitted to the photoresistor. Since the LED and photoresistor are enclosed in opaque resin, we assume that the difference of power is absorbed by the resin and converted into heat. Therefore, for convenience, the conversion from electrical to optical to micro-electrical domain is modeled as a dissipative quadripole (Fig.4). Denote v_D the LED voltage, i_D the LED current, and $P_\text{D} := i_\text{D} \, v_\text{D}$ the LED electrical power. Assume that the LED dissipative law $\mathcal{I} : v_\text{D} \mapsto i_\text{D}$ is known (e.g. from measurements or datasheets). Denote $P_{\text{opt}} := f_{\text{opt}} \, e_{\text{opt}}$ the optical power outgoing from the photoresistor. The power conversion must be passive, that is, the incoming optical power cannot be greater than the power delivered by the LED. Therefore, we choose to model the power conversion with a function f such that

$$f(P_\text{D}) + P_{\text{opt}} = 0, \quad \text{with } 0 \leq f(P_\text{D}) \leq P_\text{D}. \tag{10}$$

Assuming that $e_{\text{opt}} \neq 0$, the quadripole flow $\boldsymbol{w}$ and effort $z(\boldsymbol{w})$

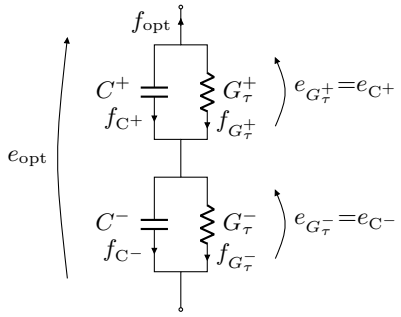

(a) *Photoresistor internal dynamics equivalent circuit schematics.*

	e_{C^+}	e_{C^-}	$f_{G_\tau^+}$	$f_{G_\tau^-}$	f_{opt}
f_{C^+}	.	.	-1	.	-1
f_{C^-}	.	.	.	-1	-1
$e_{G_\tau^+}$	1	.	.	.	.
$e_{G_\tau^-}$	.	1	.	.	.
e_{opt}	1	1	.	.	.

(b) *Corresponding PHS. Dots represent zeros.*

Figure 3: *Photoresistor internal dynamics equivalent circuit schematics and corresponding PHS.*

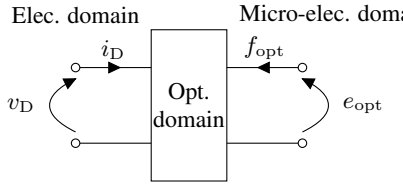

Figure 4: *Multiphysical power conversion between the LED and the photoresistor.*

can then be defined as

$$\boldsymbol{w} = [v_{\text{D}},\, e_{\text{opt}}]^\intercal\,, \quad z(\boldsymbol{w}) = \boldsymbol{\Gamma}(\boldsymbol{w})\,\boldsymbol{w} =: [i_{\text{D}},\, f_{\text{opt}}]^\intercal\,,$$

$$\text{with } \boldsymbol{\Gamma}(\boldsymbol{w}) := \underbrace{\begin{bmatrix} 0 & \frac{\mathcal{I}(v_{\text{D}})}{e_{\text{opt}}} \\ -\frac{\mathcal{I}(v_{\text{D}})}{e_{\text{opt}}} & 0 \end{bmatrix}}_{\boldsymbol{\Gamma}_{\text{antisym}}(\boldsymbol{w})} + \underbrace{\begin{bmatrix} 0 & 0 \\ 0 & \frac{\mathcal{I}(v_{\text{D}})\,v_{\text{D}} - f\left(\mathcal{I}(v_{\text{D}})\,v_{\text{D}}\right)}{e_{\text{opt}}^2} \end{bmatrix}}_{\boldsymbol{\Gamma}_{\text{sym}}(\boldsymbol{w})}. \tag{11}$$

The matrix $\boldsymbol{\Gamma}_{\text{antisym}}(\boldsymbol{w})$ encodes the (modulated) gyration from electrical to micro-electrical domain, while the (non-negative) matrix $\boldsymbol{\Gamma}_{\text{sym}}(\boldsymbol{w})$ encodes the actual power loss during the conversion. With Eq. (10), such a formulation guarantees the passivity of the quadripole, since it verifies $z(\boldsymbol{w})^\intercal \boldsymbol{w} \geq 0$ for all $\boldsymbol{w}$.

In practice, we have neither access to photoemission (from the LED), nor photoabsorption (into the photoresistor) characteristics. However, "ground truth" for the optical power P_{opt} can be obtained from measurements of the photoresistor's resistance, as will be shown in Section 5. Regarding the function f, we propose an empirical model of the form

$$f(P_{\text{D}}) = P_0\, P_{\text{D}}^{\alpha_0} + P_1\, P_{\text{D}}^{\alpha_1}, \tag{12}$$

with α_0, α_1 positive, to account for the dual-slope of the optical power as a function of the LED power observed in the logarithmic domain.

4.2. Vactrol complete model

By connecting the power converter between the LED and the photoresistor with the equivalent circuit that models the internal dynamics of the photoresistor, the vactrol (Fig. 5a) can be modeled as the equivalent circuit in Fig. 5b. The corresponding PHS equations are given in Fig. 5c.

5. IDENTIFICATION OF A VACTROL FROM MEASUREMENTS AND SIMULATION OF A SIMPLE OPTICAL COMPRESSOR

The characteristics of a VTL5C3/2 are measured to obtain the LED dissipative law, the photoresistor static resistance as a function of LED power, as well as the photoresistor's turn-on and turn-off (see [19] for a schematic of the experimental setup).

The parameters R_ℓ and R_{d} are taken from the VTL5C3/2 datasheet, and the parameters μ_0^+ and μ_0^- are set according to [20]. The remaining vactrol parameters are then estimated from measurements, in three steps.

5.1. Parameter identification for the LED

The Shockley model [21] does not capture the behavior of LEDs that are present in Vactrols accurately. Indeed, once it has reached its threshold, the LED behaves more closely as a linear resistance. Therefore, we propose a more suitable model, passive by construction, in which the LED threshold appears explicitly as a parameter. Denote v_{D} the LED voltage and i_{D} the LED current. The LED is a dissipative component of flow $\boldsymbol{w}$ and effort $z(\boldsymbol{w})$ given by

$$\boldsymbol{w} = v_{\text{D}},$$
$$z(\boldsymbol{w}) = I_s \left(\text{sp}\left(\frac{v_{\text{D}} - V_t}{V_s}\right) - \text{sp}\left(-\frac{V_t}{V_s}\right)\right) =: \mathcal{I}(v_{\text{D}}) = i_{\text{D}}, \tag{13}$$

where $\text{sp} : \; x \mapsto \ln(1 + \exp x)$ denotes the softplus function, and V_t, V_s, and I_s are positive model parameters. The voltage V_t is the LED threshold (from which it starts emitting light), and the ratio I_s/V_s corresponds to the LED conductance. Due to the fact that the sp function is increasing, and that $z(0) = 0$, this model is passive since $z(\boldsymbol{w})^\intercal \boldsymbol{w} \geq 0$ for all $\boldsymbol{w}$.

The set of parameters $\theta_{\text{D}} = [V_t,\, V_s,\, I_s]$ is estimated through a least-squares optimization. The estimated parameters are shown in Table 1. Figure 6 shows the results of the estimation compared with measurements.

5.2. Parameter identification for the photoresistor internal dynamics

To decouple the identification process, the set of parameters $\theta_{\text{LDR}} = \left[\nu_0^+,\, \nu_0^-,\, q_\tau\right]$ is estimated in isolation during turn-off, which avoids

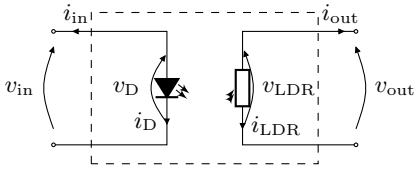

(a) *Voltage-controlled vactrol schematics.*

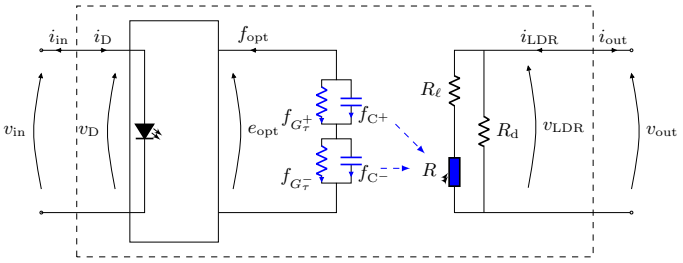

(b) *Voltage-controlled vactrol equivalent circuit schematics. The photoresistance R is modulated by the states of C^+ and C^-.*

(c) *Corresponding PHS. Dots represent zeros.*

$$
\begin{array}{cc|cccccccc|cc}
 & & \multicolumn{8}{c|}{\nabla E(\boldsymbol{x})} & & \\
 & & e_{\text{C}+} & e_{\text{C}-} & f_{G_\tau^+} & f_{G_\tau^-} & i_{\text{D}} & f_{\text{opt}} & v_{\text{LDR}} & v_{\text{in}} & i_{\text{out}} \\
\dot{\boldsymbol{x}} & f_{\text{C}+} & . & . & -1 & . & . & -1 & . & . & . \\
 & f_{\text{C}-} & . & . & . & -1 & . & -1 & . & . & . \\
\hline
 & e_{G_\tau^+} & 1 & . & . & . & . & . & . & . & . \\
 & e_{G_\tau^-} & . & 1 & . & . & . & . & . & . & . \\
\boldsymbol{w} & v_{\text{D}} & . & . & . & . & . & . & . & 1 & . \\
 & e_{\text{opt}} & 1 & 1 & . & . & . & . & . & . & . \\
 & i_{\text{LDR}} & . & . & . & . & . & . & . & . & -1 \\
\hline
\boldsymbol{y} & i_{\text{in}} & . & . & . & . & -1 & . & . & . & . \\
 & v_{\text{out}} & . & . & . & . & . & . & 1 & . & .
\end{array}
$$

Figure 5: *Voltage-controlled vactrol schematics and corresponding PHS.*

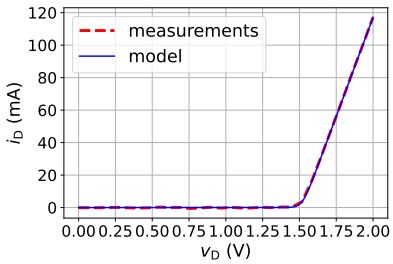

Figure 6: *LED dissipative law measurements and model.*

dependencies to the optical flow f_{opt}. Denote $R_{\text{sim}}(\theta)$ the photoresistor resistance simulated for a given set θ, using Eq. (4) with $f_{\text{opt}} = 0$ and Eq. (8). The set θ_{LDR} is obtained by fitting $R_{\text{sim}}(\theta)$ to the measured resistance through a least-squares optimization. The estimated parameters are shown in Table 1. Figure 7a shows that the resistance simulated with these parameters matches closely with the measured resistance.

5.3. Parameter identification for the power conversion law in steady state

The estimated set θ_{LDR} as well as the measured static resistance R_{LDR} as a function of LED power P_{D} can be used to provide experimental data for the optical power P_{opt}. The complete method is detailed in [19]. In this subsection, we recall the main steps but do not provide complete expressions and proofs, for brevity.

The first step is to reinject θ_{LDR} in Eq. (4) and solve for steady state $\dot{q}^+ = \dot{q}^- = 0$. This yields the relation

$$q_{st}^- = \mathcal{Q}^-(q_{st}^+), \tag{14}$$

where q_{st}^- and q_{st}^+ are the electron charge and hole charge in steady state, and $\mathcal{Q}^-$ is a function parametrized by θ_{LDR}. The second step is to substitute Eq. (14) in Eq. (8) and invert Eq. (8). We obtain the relation

$$q_{st}^+ = \mathcal{Q}^+(R_{\text{LDR}}), \tag{15}$$

where $\mathcal{Q}^+$ is a function parametrized by θ_{LDR}, μ_0^+, μ_0^-, R_{d} and R_ℓ. Finally, from Fig. 3b, we have in steady state (for the choice $C^\pm$ = 1 F, see Remark 1)

$$P_{\text{opt}} := f_{\text{opt}}\, e_{\text{opt}} = -\nu_0^- \left(q_{st}^- - q_{st}^+\right) q_{st}^- \left(q_{st}^+ + q_{st}^-\right). \tag{16}$$

By reinjecting Eqs. (14)-(15) in Eq. (16), we obtain the measured optical power P_{opt} as a function of static resistance R_{LDR}, which is itself a function of LED power P_{D}.

The set of parameters $\theta_{\text{f}} = [P_0,\ P_1,\ \alpha_0,\ \alpha_1]$ is then estimated by fitting Eq. (12) through a least-squares optimization. The estimated parameters are shown in Table 1, and Fig. 7b shows the estimation results. The simplified model matches well with the original model within the range of LED powers observed under normal use. Moreover, the passivity of the model expressed by Eq. (10) is indeed verified since $0 \leq f(P_{\text{D}}) \leq P_{\text{D}}$.

5.4. Model validation

To confirm the parameter estimation results, the photoresistor's resistance is simulated again with a non-zero optical flow, for several

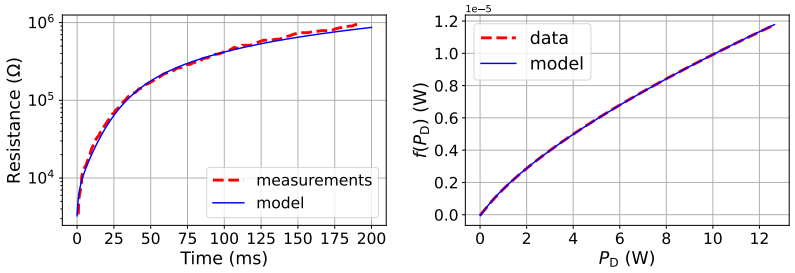

(a) *Photoresistor's turn-off measurements and model.*

(b) *Photoresistor's absorbed optical power vs LED power.*

(c) *Photoresistor's turn-on measurements and model for P_D = 70 mW.*

(d) *Photoresistor's resistance vs LED power after 800 ms.*

Figure 7: *Photoresistor characteristics: turn-off (top left), power conversion (top right), turn-on (bottom left) and resistance vs LED power after 800 ms (bottom right).*

Table 1: *Parameters for the vactrol VTL5C3/2.*

	Parameter	Value	Unit
Given	μ_0^+	4	$\mathrm{V}^{-1}{\cdot}\mathrm{s}^{-1}$
	μ_0^-	35	$\mathrm{V}^{-1}{\cdot}\mathrm{s}^{-1}$
	R_ℓ	2	Ω
	R_d	10×10^6	Ω
Estimated	q_τ	9.77×10^{-1}	C
	ν_0+	1.35×10^2	$\mathrm{C}^{-1}{\cdot}\mathrm{s}^{-1}$
	ν_0^-	1.79×10^8	$\mathrm{C}^{-1}{\cdot}\mathrm{s}^{-1}$
	P_0	-5.47×10^{-5}	W
	P_1	5.63×10^{-5}	W
	α_0	0.54	dimensionless
	α_1	0.55	dimensionless
	V_t	1.52	V
	V_s	23.16×10^{-3}	V
	I_s	5.65×10^{-3}	A

values of LED powers. The turn-on time response matches with measurements (Fig. 7c, here for P_D = 70 mW). After 800 ms of simulation (the theoretical turn-on time being 3 ms), the simulated resistance matches very closely with the measured static resistance (Fig. 7d).

5.5. Simulation of an optical compressor

The estimated parameters for the VTL5C3/2 are used to simulate a minimal optical compressor, shown in Fig. 8a. This compressor consists in a voltage divider, in which the output resistor is the photoresistor. If the output voltage is greater than the LED threshold, the LED emits light, and the photoresistor resistance drops, decreasing the output voltage in a feedback control loop [24]. The operational amplifier-based voltage follower removes the electrical coupling between the photoresistor and the LED.

For this application, we treat the voltage follower power supplies as infinite constants, so that the operational amplifier never reaches saturation. Denote v^+ the input voltage, i^+ the input current, v_o the output voltage, and i_o the output current. The voltage follower has flow $\boldsymbol{w}$ and effort $z(\boldsymbol{w})$ given by (see [22] for a complete derivation)

$$\boldsymbol{w} = \begin{bmatrix} v^+, \, i_\mathrm{o} \end{bmatrix}^\intercal, \quad z(\boldsymbol{w}) = \begin{bmatrix} 0 & 0 \\ 1 & 0 \end{bmatrix} \boldsymbol{w} =: \begin{bmatrix} i^+, \, v_\mathrm{o} \end{bmatrix}^\intercal. \tag{17}$$

Kirchhoff's laws yield the (reduced) PHS equations in Fig. 8b.

The compressor is driven with a sinusoidal voltage of the form $v_\mathrm{in} = U(t)\, \sin(2\pi\, f_0\, t)$, with $U(t)$ defined as

$$U(t) = \begin{cases} 1 & \text{if } t \leq t_0 \\ U_0 & \text{if } t_0 \leq t \leq 2\, t_0 \\ 1 & \text{if } 2\, t_0 \leq t. \end{cases} \tag{18}$$

Here, the simulation is computed with an iterative solver, namely a Newton-Raphson method [23]. Simulation results for vactrol parameters in Table 1 and simulation parameters in Table 2, are shown in Fig. 9a to Fig. 9c. We observe that the higher the input voltage, the shorter the attack and the longer the release, in agreement with the photoresistor time responses. In all cases, the attack is much sharper than the release. The compression ratio and knee can be controlled with the resistances R_1 and R_2: the higher

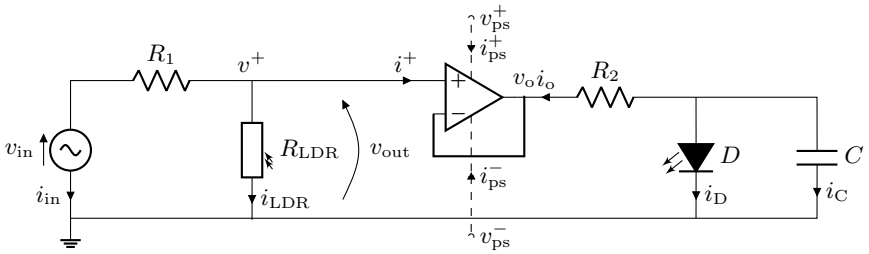

(a) *Schematics of a minimal optical compressor (OPA power supplies are dashed).*

		$\nabla E(\boldsymbol{x})$						$z(\boldsymbol{w})$				$\boldsymbol{u}$
		v_{C}	$e_{\text{C}+}$	$e_{\text{C}-}$	$f_{G_\tau^+}$	$f_{G_\tau^-}$	i_{D}	f_{opt}	i^+	v_{o}	v_{LDR}	v_{in}
$\dot{\boldsymbol{x}}$	i_{C}	$-1/R_2$	.	.	.	.	-1	.	.	$1/R_2$	.	.
	$f_{\text{C}+}$	.	.	.	-1	.	.	-1	.	.	.	.
	$f_{\text{C}-}$	.	.	.	.	-1	.	-1	.	.	.	.
$\boldsymbol{w}$	$e_{G_\tau^+}$	.	1	.	.	.	.	.	.	.	.	.
	$e_{G_\tau^-}$	.	.	1	.	.	.	.	.	.	.	.
	v_{D}	1	.	.	.	.	.	.	.	.	.	.
	e_{opt}	.	1	1	.	.	.	.	.	.	.	.
	v^+	.	.	.	.	.	.	.	.	.	1	.
	i_{o}	$1/R_2$	.	.	.	.	.	.	.	$-1/R_2$	.	.
	i_{LDR}	.	.	.	.	.	.	.	-1	.	$-1/R_1$	$1/R_1$
$\boldsymbol{y}$	i_{in}	.	.	.	.	.	.	.	.	.	$1/R_1$	$-1/R_1$

(b) *Corresponding PHS. Dots represent zeros.*

Figure 8: *Simple optical compressor schematics and corresponding PHS.*

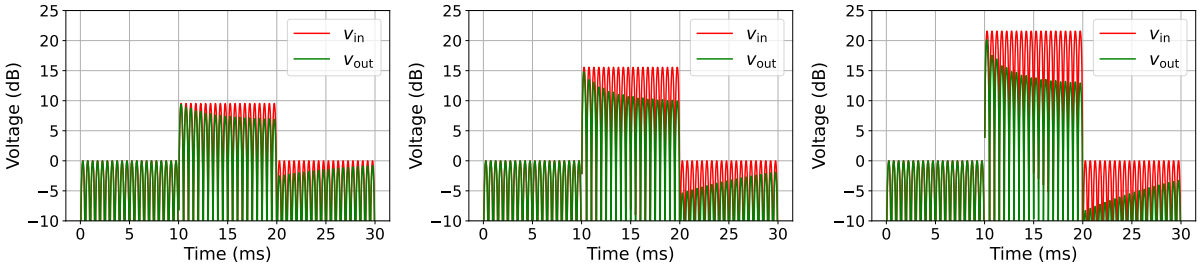

(a) *Simulation with U_0 = 3 V.*

(b) *Simulation with U_0 = 6 V.*

(c) *Simulation with U_0 = 12 V.*

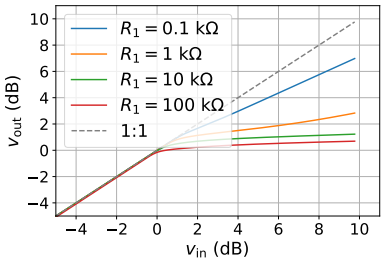

(d) *Compression ratio for different values of R_1 and fixed R_2.*

Figure 9: *Simple optical compressor simulation results.*

Table 2: *Optical compressor simulation parameters.*

Parameter	R_1 (kΩ)	R_2 (Ω)	C (μF)	U_0 (V)	f_0 (kHz)	t_0 (ms)	f_s (kHz)
Value	1	5	4.7	3-6-12	1	10	96

the ratio R_1/R_2, the higher the compression ratio and sharper the knee (Fig. 9d).

6. CONCLUSION

In this paper, we proposed a dynamic, multiphysical and power-balanced model for the vactrol, as a port-Hamiltonian system. First, we modeled the photoresistor. Its internal dynamics were obtained from the study of doping mechanisms in semiconductors. Then, we addressed the nonlinear optical coupling between the LED and the photoresistor. A law for this coupling was derived from the photoresistor's static resistance as a function of the LED's electrical power.

The model's parameters were successfully estimated from measurements of a real vactrol. Simulations using the estimated parameters closely match with measured dynamic and static characteristics. Finally, the model was implemented in order to simulate a minimal optical compressor. The simulated attack and release times are program-dependent, as expected in such compressors.

Regarding ongoing work, the model is being implemented in complex circuits that are closer to real optical compressors, and tested against real audio signals for a more complete assessment.

7. REFERENCES

[1] Lynn Fuston. A history of the Teletronix LA-2A leveling amplifier.

[2] Manley. `https://www.manley.com/pro/melpp`.

[3] *Photoconductive cells and analog optoisolators (Vactrols)*. Perkin Elmer Optoelectronics, 2001.

[4] Julian Parker and Stephano D'Angelo. A digital model of the Buchla lowpass-gate. In *Proc. Int. Conf. Digital Audio Effects (DAFx-13), Maynooth, Ireland*, pages 278–285, 2013.

[5] Felix Eichas and Udo Zölzer. Modeling of an optocoupler-based audio dynamic range control circuit. In *Novel Optical Systems Design and Optimization XIX*, volume 9948, page 99480W. International Society for Optics and Photonics, 2016.

[6] Alec Wright, Vesa Välimäki, et al. Grey-box modelling of dynamic range compression. In *Proc. Int. Conf. Digital Audio Effects (DAFx-22), Vienna, Austria*, pages 304–311, 2022.

[7] Riccardo Simionato and Stefano Fasciani. Deep learning conditioned modeling of optical compression. In *Proc. Int. Conf. Digital Audio Effects (DAFx-22), Vienna, Austria*, pages 288–295, 2022.

[8] Nicolas Lopes and Thomas Hélie. Energy balanced model of a jet interacting with a brass player's lip. *Acta Acustica united with Acustica*, 102(1):141–154, 2016.

[9] Antoine Falaize and Thomas Hélie. Passive simulation of the nonlinear port-Hamiltonian modeling of a Rhodes piano. *Journal of Sound and Vibration*, 390:289–309, 2017.

[10] B. M. Maschke, A. J. van der Schaft, and P. Breedveld. An intrinsic Hamiltonian formulation of network dynamics: Non-standard Poisson structures and gyrators. *Journal of the Franklin institute*, pages 923–966, 1992.

[11] Vincent Duindam, Alessandro Macchelli, Stefano Stramigioli, and Herman Bruyninckx. *Modeling and control of complex physical systems: The port-Hamiltonian approach*. Springer Science & Business Media, 2009.

[12] A. J. van der Schaft, Dimitri Jeltsema, et al. Port-Hamiltonian systems theory: An introductory overview. *Foundations and Trends in Systems and Control*, 1(2-3):173–378, 2014.

[13] Antoine Falaize and Thomas Hélie. Passive guaranteed simulation of analog audio circuits: A port-Hamiltonian approach. *Applied Sciences*, 6(10):273, 2016.

[14] Rémy Müller. *Time-continuous power-balanced simulation of nonlinear audio circuits: Realtime processing framework and aliasing rejection*. PhD thesis, Sorbonne Université, 2021.

[15] Timothy A. Bigelow. Power and energy in electric circuits. In *Electric Circuits, Systems, and Motors*, pages 105–121. Springer, 2020.

[16] Marius Grundmann. *Physics of semiconductors*, volume 11. Springer, 2010.

[17] U.V. Desnica. Doping limits in II–VI compounds—Challenges, problems and solutions. *Progress in crystal growth and characterization of materials*, 36(4):291–357, 1998.

[18] Arthur Evan Iverson. *The mathematical modeling of time-dependent photoconductive phenomena in semiconductors*. PhD thesis, The University of Arizona, 1987.

[19] Judy Najnudel. *Power-Balanced Modeling of Nonlinear Electronic Components and Circuits for Audio Effects*. PhD thesis, Sorbonne Université, 2022.

[20] WE Spear and J Mort. Electron and hole transport in CdS crystals. *Proceedings of the Physical Society (1958-1967)*, 81(1):130, 1963.

[21] William Shockley. The theory of p-n junctions in semiconductors and p-n junction transistors. *Bell System Technical Journal*, 28(3):435–489, 1949.

[22] Rémy Müller and Thomas Hélie. A minimal passive model of the operational amplifier: Application to Sallen-Key analog filters. In *Proc. of the 22nd Int. Conference on Digital Audio Effects*, 2019.

[23] Peter Deuflhard. *Newton methods for nonlinear problems: Affine invariance and adaptive algorithms*, volume 35. Springer Science & Business Media, 2011.

[24] Jonathan S Abel and David P Berners. On peak-detecting and rms feedback and feedforward compressors. In *Audio Engineering Society Convention 115*. Audio Engineering Society, 2003.